Optical coherence tomography for dynamic axial correction of an optical end-effector for robot-guided surgical laser ablation

Jamil Jivraj
Chaoliang Chen
Dexter Barrows
Victor X. D. Yang

SPIE.

Optical coherence tomography for dynamic axial correction of an optical end-effector for robot-guided surgical laser ablation

Jamil Jivraj,[a] **Chaoliang Chen,**[a] **Dexter Barrows,**[b] **and Victor X. D. Yang**[a,c,*]
[a]Ryerson University, Department of Electrical and Computer Engineering, Biophotonics and Bioengineering Laboratory, Toronto, Canada
[b]7D Surgical Inc., Toronto, Canada
[c]Sunnybrook Health Sciences Centre, Department of Neurosurgery, Toronto, Canada

Abstract. Robot-guided laser ablation for surgical applications potentially offers many advantages compared to by-hand mechanical tissue cutting. However, given that tissue can be rough and/or uneven, ablation quality can be compromised if the beam waist deviates significantly from the target tissue surface. Therefore, we present a method that uses optical coherence tomography (OCT) for dynamic refocusing of robot-guided surgical laser ablation. A 7-DOF robotic manipulator with an OCT-equipped optical payload was used to simulate robotic guided laser osteotomy. M-mode OCT feedback is used for continuous surface detection to correct for axial deviations along the ablation path due to surface nonuniformity. We were able to show that such a correction scheme could maintain the beam waist within the depth of focus for surface variation as aggressive as 45 deg with feed rates up to 1 mm/s. Strategies for implementation in surgical and nonsurgical applications are examined. © *The Authors. Published by SPIE under a Creative Commons Attribution 4.0 Unported License. Distribution or reproduction of this work in whole or in part requires full attribution of the original publication, including its DOI.* [DOI: 10.1117/1.OE.58.5.054106]

Keywords: optics; photonics; light; lasers; dynamic focus; ablation.

Paper 190216 received Feb. 17, 2019; accepted for publication May 16, 2019; published online May 31, 2019.

1 Introduction

For the purposes of laser osteotomy, maintenance of the beam waist at the surface of the bone in real-time is critical for optimal ablation quality. The challenge is that unlike in most industrial laser material processing applications, most bones do not have large surfaces that are smooth and flat. Also, minute variations along the surface that can still affect ablation quality are not always fully captured using current medical imaging modalities, given resolution constraints; this means that adaptation along a surface using prior knowledge of surface variations may not be fully effective. Therefore, it would be quite advantageous for a laser osteotomy system to make continuous, real-time, sub-millimeter adaptations along the optical axis in order to maintain beam focus along uneven surfaces.

Several techniques exist for laser materials processing to maintain focus of the workpiece.[1] Field effect sensors and contact sensors have been demonstrated with success in the processing of certain materials. However, in the context of surgery, these sensors can not perform adequately. Field effect sensors rely on inductive or capacitive interaction between the workpiece and the sensor to determine axial distance. These methods work for metallic work pieces, but they can only be used between laser pulses since the high intensity of the electric field of the laser pulse affects distance measurements. Contact sensors would not be suitable for applications of laser tissue ablation because of their innate negation of the noncontact benefit of using laser light to cut tissue. Various optical sensing methods have been reported to measure workpiece distance along the optical axis in

real-time. Techniques involving monitoring of the laser spot diameter using image sensors have also been developed[2,3] but may not perform well on irregular surfaces, defocusing direction may remain ambiguous, and marking the specimen by firing the machine beam in order to make a spot measurement may cause unwanted damage to the target. Hand et al.[4] developed a technique that redirected a fraction of the process-generated light into a separate optical path for analysis of the chromatic aberrations to determine focal error. Cao et el. recently developed methods involving a diffractive beam samplers,[5] as well as hole-mask, separate interrogation source,[6] and multiple intermediate bulk-optic elements and a CCD to place the target in the focus of the machining beam. By monitoring the change in diffraction pattern on the CCD, these techniques allow for determination of the workpiece position along the optical axis and the direction of defocusing.

We explore the use of OCT to guide a robot-guided laser ablation objective payload over a target for surgery. OCT has been used to guide other types of surgical payloads. Studies have been carried out by Yu et al.[7–10] for OCT guidance of retinal surgery payloads. B-mode OCT feedback was used to track the tips of various instruments (micropipette,[10] grippers,[9] and injection pipette[8]), in real-time. Sub-millimeter tracking accuracy was reported while using a Steward–Gough robotic platform. Cheon et al. explored a similar application in ophthalmic surgery where OCT was used to guide a needle to a precise depth into a bovine eye.[11] These studies prove that OCT can be successfully used in real-time guidance of various robotic surgical payloads.

In this paper, we propose the use of m-mode OCT as a feedback mechanism for dynamic axial adjustment of the payload of a 7-DOF robot with respect to uneven and rough/nonplanar surfaces. The peak of the OCT signal, which

*Address all correspondence to Victor X. D. Yang, E-mail: vyang@ee.ryerson.ca

defines the surface, is used for correcting the offset distance along the optical axis between the robot-mounted objective lens and surface of the target. Given that OCT innately has the ability to measure displacement along the optical axis, ambiguity in defocusing direction is removed using this method. The application of this technique is for ablation of bone during surgery via robotic path guidance. The technique proposed in this paper can be easily integrated into various surgical and nonsurgical ablation schemes. Figure 1 shows two widely reported schemes of dual-wavelength beam combination that has been used for ablation process monitoring and control using OCT. Figure 1(a) shows the most prevalent beam combination method, which uses a dichroic element to guide both free-space beam paths into a single set of objective optics.[13–15] Figure 1(b) shows a method that maintains a single fiber output path for both beams by combining the ablation source (in this case, a fiber laser) directly into the sample arm of the OCT system, reducing the amount of bulk optic elements at or near the output.[12]

Both methods can be easily used to design an optical payload for robot-guided ablation, as shown in Fig. 2. It is important to note that any method that uses different wavelengths for ablation and interrogation with a single set of objective optics will have a shift along the axial direction between the waists of both beams. This easily measurable offset must be taken into account so that the ablation beam waist is always kept at the specimen surface.

2 System Description

2.1 *Hardware*

2.1.1 *Robotic manipulator*

The robotic manipulator used in this system is the IIWA, manufactured by KUKA AG. The IIWA is a 7-DOF anthropomorphic manipulator designed to work in close proximity with humans, such as in a surgical setting. The robot has a quoted maximum payload weight of 14 kg and
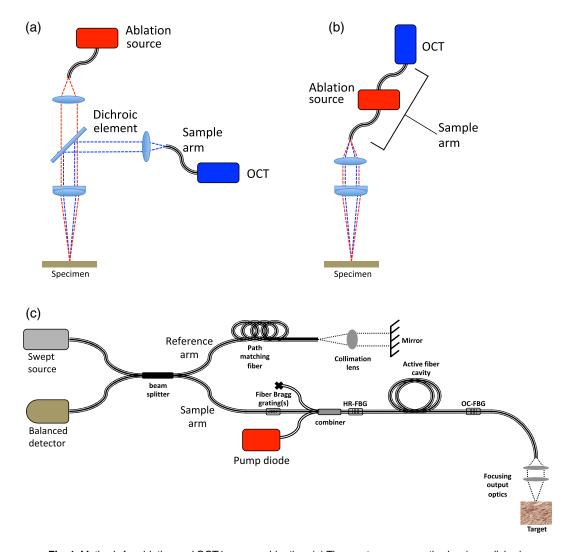

Fig. 1 Methods for ablation and OCT beam combination. (a) The most common method, using a dichroic mirror to combine the high-powered ablation beam with relatively low-powered OCT beam. The wavelength-specific transmissivity of the dichroic element prevents high-powered ablation light from following the beam path of the OCT system. (b) A method that involves a fiber laser to be built directly into the sample arm of the OCT system, as proposed by Jivraj et al.[12] (c) The method shown in (b) in more detail. The ablation laser built into the sample arm of the OCT system was a single-mode Yb-doped fiber laser with $\lambda_0 = 1064$ mm, 50 kHz repetition rate, 160 ns pulse duration, $P_{avg} = 3.35$ W, and $P_{peak} = 419$ W.
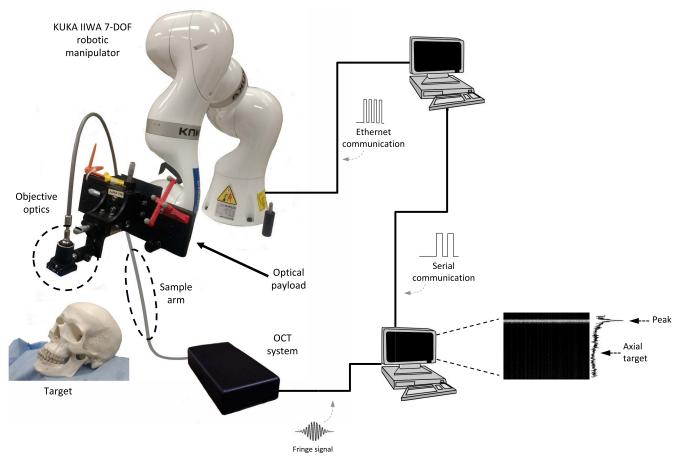
Fig. 2 System diagram. The 7-DOF manipulator carries optical payload (with objective optics) over target. Feedback of axial position over target's surface is measured in real-time via OCT and correction is sent to the robot over high-speed serial communication. The two elements highlighted in dashed lines (objective optics and delivery fiber) show where either of the two method of beam combination explained in Fig. 1 would take place.

a positioning accuracy of ± 0.1 mm.[16] The robot was sent axial position information in real-time via ethernet communication protocol using a desktop computer. The update period between the robot and the computer was ~500 ms.

2.1.2 *Optical payload and beam delivery*

The sample arm beam of the OCT system is delivered via fiber to a Thorlabs F810APC-1064 doublet collimator. The collimated light is then focused through a Thorlabs AC-254-150C achromatic doublet lens. The measured spot size d_o, depth of focus L_d, and focal length L_f are 48 μm, 2.1 mm, and 146 mm, respectively; Fig. 3 shows a physical summary. The focusing optics are attached to the mounting flange of the robot (corresponding to the seventh degree of freedom) using an optical breadboard. The location of the focal spot is programmed to be the tool center point of the end-effector.

2.1.3 *Swept-source OCT system*

The OCT system consisted of a 1310-nm centered swept wavelength MEMS laser (Santec HSL-20-50-S) with a bandwidth of 105 nm, sweep rate of 50 kHz, and (measured) average power output of 18 mW. A fiber-based Michelson interferometer (50/50 coupling ratio) and a Thorlabs PDB415C 100 MHz balanced detector were used. The signal was acquired using an Alazartech ATS9350 digitizer card.
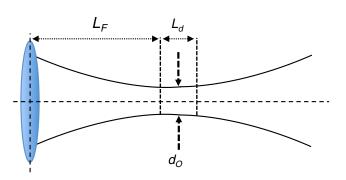

Fig. 3 Anatomy of a focused Gaussian beam. Depth of focus denotes planes along optical axis at which beam area is twice that of the area at beam waist. $L_d/2$ denotes Rayleigh length. It is typically desirable to maintain the specimen surface at the beam waist.

The entire OCT system was constructed using SMF-28 fiber. Figure 4(a) shows the diagram for the OCT system and Fig. 4(b) shows its point spread function (PSF). Peak detection of the Fourier transformed interference fringe signal (acquired by the balanced detector) was used to determine the axial offset of the surface of the target; this information was processed in real-time using a desktop computer using in-house developed software.
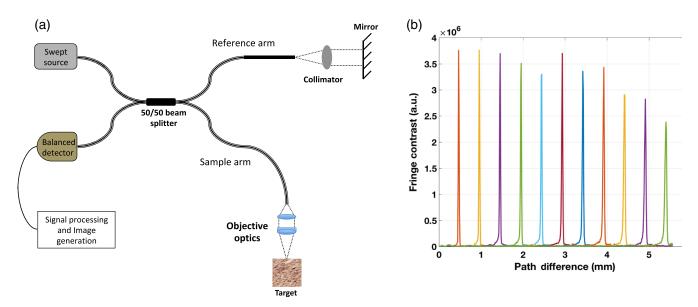
(a)

(b)

Fig. 4 (a) Schematic of fiber-based swept-source OCT system. (b) PSF of OCT system. Axial resolution = 9 μm.

2.1.4 Explanation of elimination of defocusing direction ambiguity

Given the nature of the swept-source OCT interference fringe signal captured by the photodetector, defocusing directional ambiguity is eliminated. The frequency composition of the fringes is depth-dependant—higher frequencies are proportional to larger optical path difference. Figure 5 shows this
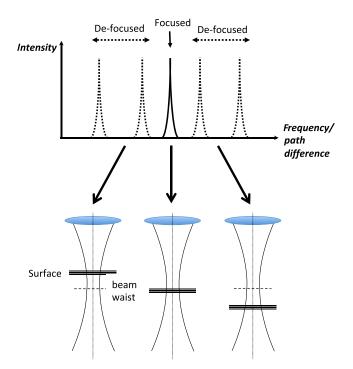
concept in greater detail. The plot in the diagram shows the fringe signal after the Fourier transform; the sharp peaks represent the surface reflection. The further the peak travels along the frequency axis, the larger the optical path difference, meaning the further the surface is away from the payload along the optical axis. Any point along the frequency axis can be arbitrarily chosen as the target position; typically this is where the beam waist is placed in relation to the target. Any deviation from this chosen position can be easily compensated for by determining the difference between the current position along the frequency axis and the desired, focused position.

2.1.5 System integration

A high-speed serial communication link between the two desktop computers was established so that OCT-acquired
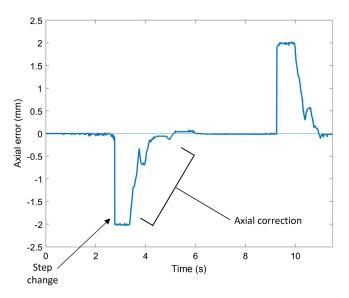

Fig. 5 Elimination of ambiguity in defocusing direction. The plot represents the fringe signal post-Fourier transform. The peak represents the position of the target surface along the optical axis. The frequency is directly proportional to the optical path difference; therefore, position of the peak along the frequency axis represents the absolute position of the surface along the optical axis.

Fig. 6 Response of system correction to step change in the axial direction.
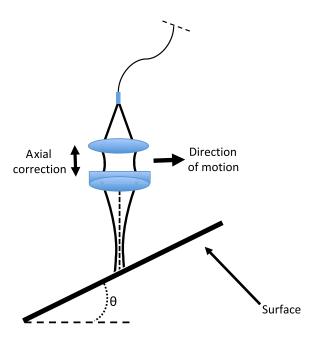
Fig. 7 Schematic of slope progression experiment. θ represents the angles that the surface was positioned to.

axial peak position could be relayed in real-time to the computer commanding the manipulator. The workflow for the system was designed as follows:

1. Acquire the interferogram from the photodetector.
2. Perform signal filtering and Fourier transform to attain depth-dependant frequency spectrum.
3. Perform peak detection and check if the peak has moved from initial position (taken to be 0 mm); if the peak has moved, send the robot the updated axial correction to bring it back to 0 mm position.

3 Experiments and Results

A series of experiments were performed in order to characterize the mean distance at which the robot was able to position the beam waist relative to the surface of a target while the target was linearly translated. The goal was to maintain the surface of the target within the depth of focus, as close to the beam waist as possible. The axial positions were recorded in real-time using m-mode OCT imaging.
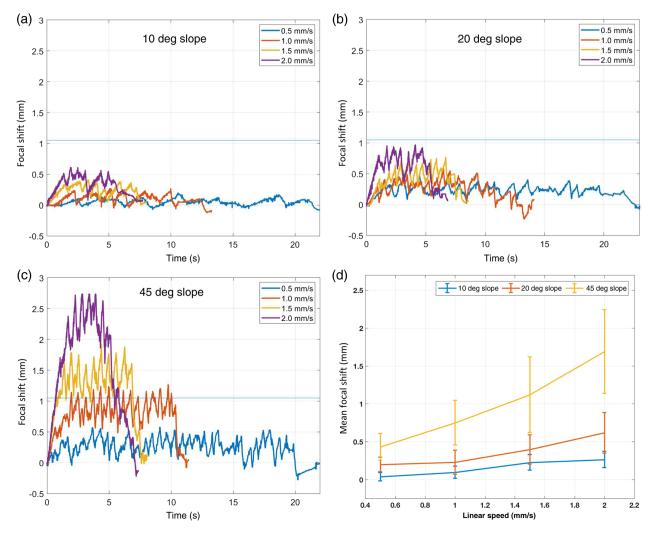

Fig. 8 Phantom experiments summarizing tracking error versus linear speed and slope. (a–c) M-mode tracking error at 10 deg, 20 deg, and 45 deg surface incline, respectively. Blue line demarcates Rayleigh length. (d) Mean of tracking error experiments.

3.1 Step Response

The robot was made to adapt to a step elevation change of 2 mm, which represents the most aggressive input change possible; with the m-mode system response shown in Fig. 6. The figure shows the surface at axial error at 0 mm, meaning that the surface is at its intended target axial position. The target surface is dropped 2 mm, showing the negative step change in Fig. 6; after a short dwell period, corrective action is initiated, and the robot end effector is moved along the optical axis until the surface of the target is brought back to 0 mm axial error. The process is then repeated with a positive step change. The total response time (10% to 90% definition) of 1.3 s was found, which corresponds to a total response rate of 0.77 Hz.

3.2 Axial Correction on Sloped Progression

To characterize axial adaptation performance along a gradual elevation change, a surface sloped at various angles was used as a target, as shown in Fig. 7. The optical payload was linearly translated 10 mm laterally at four different linear velocities (0.5, 1.0, 1.5, and 2.0 mm/s) relative to a surface at three different slopes (10 deg, 20 deg, and 45 deg). M-mode OCT data were recorded to show axial deviation from the target similar to Fig. 6; this is shown in Fig. 8). As expected, the increase in slope angle and linear velocity corresponded to a larger cumulative axial error. It was also seen that at the most aggressive slope, 45 deg, linear speeds of up to 1.0 mm/s could be maintained with the axial error still staying below the Rayleigh length of the focusing optics.

At 1.5 mm/s and higher, the axial error began to drift outside the Rayleigh length.

3.3 Experiment on Skull Phantom

A 1:1 scale human skull phantom was used as a target to characterize the mean axial tracking error. This allowed for a very close approximation of the system performance characterization for a real world osteotomy scenario. The phantom was placed such that the transverse plane of the skull was positioned perpendicularly to the optical axis of the objective lens, as shown in Fig. 9. The payload was moved along the sagittal suture, simulating a cranial osteotomy. The mean tracking error from the beam waist was found to be -0.02 and -0.2 mm for 0.5 and 1.0 mm/s linear velocity, respectively.

4 Discussion and Conclusions

We have shown that OCT is a viable method for surface detection and dynamic refocusing using a robotic manipulator. The technique developed is able to keep the target within the depth of focus for the objective lens at surface inclines as aggressive as 45 deg for linear velocities of up to 1.0 mm/s. For less aggressive slopes, dynamic focusing was successful for linear velocities of up to 2.0 mm/s. This agrees well actual mechanical bone cutting feed rates, such as those explored by Davidson and James[17] (up to 5 mm/s). This technique can be useful when the surface profile is not quantified beforehand, or if the surface tends to shift during ablation, i.e., during patient breathing. As well, this technique is able to maintain focus along a surface with variations that are
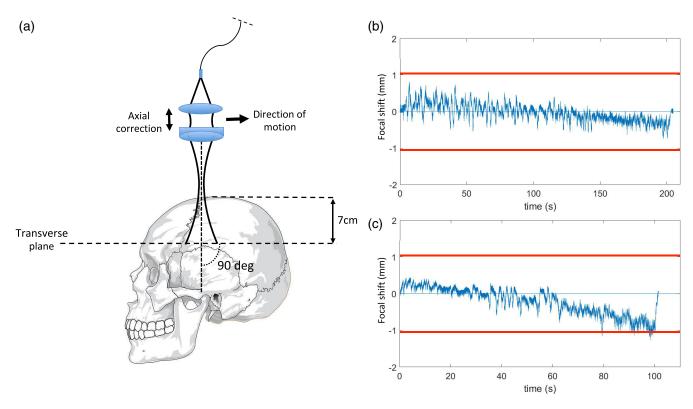

Fig. 9 (a) Diagram showing axial adaptation on a skull phantom target. Experiment is executed over the transverse medial suture. Total axial height change is 7 cm over the 10 cm linear translation. (b, c) Axial tracking error results over transverse suture of the skull phantom for 0.5 and 1.0 mm/s, respectively. Red lines represent Rayleigh lengths.

irresolvable using most medical imaging modalities. The simplicity of this technique lends well to integration into existing ablation systems where OCT is integrated in-line for depth monitoring.[13,12,18,19] Also, we have shown that this type of correction is possible without the use of galvo-scanners for b-mode scanning, thereby reducing potentially maintaining a minimum payload complexity to a single collimating lens and single objective lens.

As seen in Sec. 3, mean accuracy during increasingly aggressive slope of the surface significantly improved with the reduction of speed. This means that the axial error can be significantly improved if the feed-rate of the workpiece can be dynamically modulated based on axial deflection/incline as ascertained by OCT surface feedback.

Future steps in this work entail increasing the system loop-rate so that adaptation can occur faster, thereby potentially adapting to high-frequency surface artifacts and increasing the feed rate of the workpiece.

Acknowledgments

References

1. W. Steen and J. Mazumder, *Laser Material Processing*, Springer Science and Business Media (2010).
2. B. X. Cao et al., "Design and performance of a focus-detection system for use in laser micromachining," *Micromachines* **7**(1), 2 (2016).
3. T. Grosjean and D. Courjon, "Smallest focal spots," *Opt. Commun.* **272**(2), 314–319 (2007).
4. D. Hand et al., "Optical focus control system for laser welding and direct casting," *Opt. Lasers Eng.* **34**, 415–427 (2000).
5. B. X. Cao et al., "Real-time detection of focal position of workpiece surface during laser processing using diffractive beam samplers," *Opt. Lasers Eng.* **86**, 92–97 (2016).
6. B. X. Cao et al., "In-situ real-time focus detection during laser processing using double-hole masks and advanced image sensor software," *Sensors* **17**, 1540 (2017).
7. H. Yu et al., "Design, calibration and preliminary testing of a robotic telemanipulator for OCT guided retinal surgery," in *IEEE Int. Conf. Rob. and Autom. (ICRA)*, IEEE (2013).
8. K. M. Joos and J.-H. Shen, "Preliminary design and evaluation of a b-scan OCT-guided needle," *Photonics* **1**(3), 260–266 (2014).
9. H. Yu et al., "Evaluation of microsurgical tasks with OCT-guided and/or robot-assisted ophthalmic forceps," *Biomed. Opt. Express* **6**, 457–472 (2015).
10. H. Yu et al., "Calibration and integration of b-mode optical coherence tomography for assistive control in robotic microsurgery," *IEEE/ASME Trans. Mechatron.* **21**, 2613–2623 (2016).
11. G. W. Cheon et al., "Accurate real-time depth control for CP-SSOCT distal sensor based handheld microsurgery tools," *Biomed. Opt. Express* **6**(5), 1942–1953 (2015).
12. J. Jivraj et al., "Smart laser osteotomy: integrating a pulsed 1064 nm fiber laser into the sample arm of a fiber optic 1310 nm OCT system for ablation monitoring," *Biomed. Opt. Express* **9**(12), 6374–6387 (2018).
13. S. A. Boppart et al., "High-resolution optical coherence tomography-guided laser ablation of surgical tissue," *J. Surg. Res.* **82**(2), 275–284 (1999).
14. P. J. Webster et al., "Coaxial real-time metrology and gas assisted laser micromachining: process development, stochastic behavior, and feedback control," *Proc. SPIE* **7590**, 759003 (2010).
15. Y. Ji, "Inline coherent imaging applied to laser micromachining," Master's Thesis (2014).
16. KUKA-Roboter-GmbH, "Kuka senstive robotics LBR IIWA," *PDF Brochure* (2017).
17. S. R. Davidson and D. F. James, "Drilling in bone: modeling heat generation and temperature distribution," *J. Biomech. Eng.* **125**(3), 305–314 (2003).
18. P. J. Webster et al., "Automatic real-time guidance of laser machining with inline coherent imaging," *J. Laser Appl.* **23**(2), 022001 (2011).
19. J. Jivraj et al., "Coaxial cavity injected OCT and fiber laser ablation system for real-time monitoring of ablative processes," *Proc. SPIE* **9305**, 930505 (2015).

Jamil Jivraj is a PhD candidate in electrical and computer engineering at Ryerson University. He received his MASc degree in electrical and computer engineering (legged robotics focus) and his BEng degree in electrical engineering both from Ryerson University. His research interests include mechatronic devices for surgery, optical coherence tomography, laser ablation of tissue, and medical applications of photonics.

Chaoliang Chen received his BS degree in optoelectronic engineering in 2011 and PhD in optical engineering in 2016, respectively, from Nanjing University of Science and Technology. He is currently undertaking post doctoral research at Sunnybrook Research Institute and Ryerson University. His research includes biomedical optical imaging, such as optical coherence tomography.

Dexter Barrows is a software developer working at 7D Surgical, building software powering the next generation of surgical navigation systems. He has previously worked at the Biophotonics and Bioengineering Laboratory (BBL) at Ryerson University and Sunnybrook Health Sciences Centre, developing algorithms and software for GPU-accelerated medical image processing, Doppler optical coherence tomography, and computational anatomy segmentation. He holds master's and bachelor's degrees in applied mathematics with concentrations in scientific computing and numerical methods.

Victor X. D. Yang holds an MASc in ELCE (1998) from the University of Toronto, where he also completed the MD-PhD (medical biophysics) program in 2006. He is a professor of ELCE at Ryerson University, a staff neurosurgeon at Sunnybrook Health Sciences Centre, and a senior scientist in Brain Sciences and Physical Sciences at Sunnybrook Research Institute. His research includes surgical navigation, multimodality intraoperative guidance, endovascular imaging, and minimally invasive carotid disease and stroke therapeutics.